Quantum correlations and spatial localization in one-dimensional ultracold bosonic mixtures

2014 New J. Phys. 16 103004

(http://iopscience.iop.org/1367-2630/16/10/103004)

New Journal of Physics
The open access journal at the forefront of physics
Deutsche Physikalische Gesellschaft DPG | IOP Institute of Physics

Quantum correlations and spatial localization in one-dimensional ultracold bosonic mixtures

M A García-March[1], B Juliá-Díaz[1,2], G E Astrakharchik[3], Th Busch[4], J Boronat[3] and A Polls[1]

[1] Departament d'Estructura i Constituents de la Matèria, Universitat de Barcelona, 08028 Barcelona, Spain
[2] ICFO-Institut de Ciències Fotòniques, Parc Mediterrani de la Tecnologia, 08860 Barcelona, Spain
[3] Departament de Física i Enginyeria Nuclear, Campus Nord B4, Universitat Politècnica de Catalunya, E-08034 Barcelona, Spain
[4] Quantum Systems Unit, OIST Graduate University, Okinawa, Japan

Received 3 June 2014, revised 2 September 2014
Accepted for publication 11 September 2014
Published 7 October 2014

New Journal of Physics **16** (2014) 103004

doi:10.1088/1367-2630/16/10/103004

Abstract

We present the complete phase diagram for one-dimensional binary mixtures of bosonic ultracold atomic gases in a harmonic trap. We obtain exact results with direct numerical diagonalization for a small number of atoms, which permits us to quantify quantum many-body correlations. The quantum Monte Carlo method is used to calculate energies and density profiles for larger system sizes. We study the system properties for a wide range of interaction parameters. For the extreme values of these parameters, different correlation limits can be identified, where the correlations are either weak or strong. We investigate in detail how the correlations evolve between the limits. For balanced mixtures in the number of atoms in each species, the transition between the different limits involves sophisticated changes in the one- and two-body correlations. Particularly, we quantify the entanglement between the two components by means of the von Neumann entropy. We show that the limits equally exist when the number of atoms is increased for balanced mixtures. Also, the changes in the correlations along the transitions among these limits are qualitatively similar. We also show that, for imbalanced mixtures, the same limits with similar transitions exist. Finally, for strongly imbalanced systems, only two limits survive, i.e., a miscible

limit and a phase-separated one, resembling those expected with a mean-field approach.

Keywords: bosonic mixtures, Tonks–Girardeau gas, few-atom systems, macroscopic superpositions

1. Introduction

The fascinating physics of interpenetrating superfluids has recently become a topic of great interest due to the experimental realization of multi-component, atomic Bose–Einstein condensates [1–5]. In the weakly interacting regime, these mixtures are well described by coupled mean-field Gross–Pitaevskii equations (GPEs), and within this framework, processes that lead to phase separation are well described [6–14].

While mean-field theories allow us to study weakly correlated systems, it is also important and interesting to examine quantum mixtures in strongly correlated regimes. In these regimes, analytic solutions can often be obtained only in limiting cases. Rather appealing results occur in strongly correlated regimes when the dimensionality is reduced. For quasi-one-dimensional (1D) gas mixtures, one finds that the Luttinger liquid theory predicts many interesting effects, which include de-mixing for repulsive interactions or spin-charge separation analogous to that found in 1D electronic quantum systems [15–18]. Other relevant effects include the presence of polarized ground states, which allow us to view the relative spatial oscillations as spin waves [19–23] and which have been experimentally observed [24–26].

Very strong correlations for single-component bosons are realized in the Tonks–Girardeau (TG) gas [27–29], which was recently observed experimentally [34, 35]. Bosonic mixtures in the strongly interacting limit have features common with the TG gas, and their ground-state wavefunction can be obtained analytically in certain interaction limits [36–38]. Experimental advances on Feshbach and confinement-induced resonances in recent years have made it possible to control both the intra-species interactions and the inter-species interactions over a wide range of parameters [39–41]. In the strongly interacting limit, a number of relevant phenomena have been described, including phase separation [15–17, 42], composite fermionization [43–45], a sharp crossover between both limits [46], and quantum magnetism [47].

In this work we focus on mixtures where the number of atoms is small. The recent successful experimental trapping of ensembles of a few atoms [48–52] has inspired an intense theoretical effort [53–67], and very recently even systems with SU(N) symmetry and $N > 2$ have been experimentally realized [68]. For mixtures of a few atoms, direct diagonalization methods [31, 42, 45] can be used together with other numerical methods efficient for larger numbers of atoms, like multiconfigurational Hartree–Fock methods (MCTDH) [70], density functional theory (DFT) [44], or quantum diffusion Monte Carlo (DMC) [69]. In the present work, we use direct numerical diagonalization to study the ground-state properties of a mixture of ultracold bosons confined in a 1D trap over a wide range of correlations regimes, determined by the scattering properties between the atoms. These are supplemented by DMC calculations to confirm trends for systems with larger particle numbers. While the extreme cases in which all correlations are either weak or strong are well known, here we calculate and discuss the full phase diagram and especially the transitions between the different regimes.

We study the ground-state wavefunction and pay particular attention to the one- and two-body correlations in the extreme limits and across the transitions between them. The quantum correlations between both components are characterized by means of the von Neumann entropy. This allows us to show that close to the crossover between the *composite fermionization* and *phase separation*, the ground state exhibits strong correlations between the two bosonic components.

Our paper is organized as follows. In section 2 we introduce the model Hamiltonian and a general analytical ansatz for the ground-state wavefunction. Focusing first on balanced mixtures, we discuss in section 3 the ground-state properties in terms of the densities, the coherence, the energies, the one- and two-body correlations, and the von Neumann entropy. In section 4, we then present results on how the ground-state properties change when one component is larger than the other, and finally summarize all our results in section 5.

2. Model hamiltonian

Let us consider a mixture of two bosonic components, A and B, with a small, fixed number of atoms in each component, $N_{\rm A}$ and $N_{\rm B}$. We assume that the two components are two different hyperfine states of the same atomic species of mass m and that they are trapped in the same, 1D parabolic potential $V(x) = \frac{1}{2}m\omega^2 x^2$. At low temperatures, all scattering processes between the atoms are assumed to be described by contact interactions $v_{\rm int}^{\rm A} = g_{\rm A}\delta(x_j - x_{j'})$, $v_{\rm int}^{\rm B} = g_{\rm B}\delta(y_j - y_{j'})$, and $v_{\rm int}^{\rm AB} = g_{\rm AB}\delta(x_i - y_j)$, where the positions of atoms of species A(B) are given by the coordinates $x_j(y_j)$. The 1D intra- and inter-species coupling constants $g_{\rm A(B)}$ and $g_{\rm AB}$ are assumed to be tunable independently by means of confinement-induced resonances [39]. We will restrict our study to repulsive interactions. The many-body Hamiltonian is $\hat{\mathcal{H}} = \hat{\mathcal{H}}_{\rm A} + \hat{\mathcal{H}}_{\rm B} + \hat{\mathcal{H}}_{\rm int}$, with:

$$\begin{aligned}
\hat{\mathcal{H}}_{\rm A} &= \sum_{j=1}^{N_{\rm A}}\left[-\frac{\hbar^2}{2\,m}\frac{\partial^2}{\partial x_j^2} + V(x_j)\right] + \sum_{j<j'}^{N_{\rm A}} v_{\rm int}^{\rm A}(x_j, x_{j'}),\\
\hat{\mathcal{H}}_{\rm B} &= \sum_{j=1}^{N_{\rm B}}\left[-\frac{\hbar^2}{2\,m}\frac{\partial^2}{\partial y_j^2} + V(y_j)\right] + \sum_{j<j'}^{N_{\rm B}} v_{\rm int}^{\rm B}(y_j, y_{j'}),\\
\hat{\mathcal{H}}_{\rm int} &= \sum_{j=1}^{N_{\rm A}}\sum_{j'=1}^{N_{\rm B}} v_{\rm int}^{\rm AB}(x_j - y_{j'}).
\end{aligned} \tag{1}$$

There are three coupling constants $g_{\rm A}$, $g_{\rm B}$, $g_{\rm AB}$, each of them ranging from $g = 0$ for the ideal Bose gas interaction to $g \to \infty$ for a strong Tonks–Girardeau interaction. This defines eight limits schematically shown in figure 1. The composite fermionization limit is reached when $g_{\rm AB} \to \infty$, with the other coupling constants vanishing [43–45]. We termed TG–BEC gas a system with one of the intra-species coupling constants large, while other coupling constants vanish [42]. If one of the intra-species coupling constants, together with the inter-species coupling constant, are large, the phase separation limit is reached [15–17, 42]. Finally, if all coupling constants tend to infinity, the wavefunction is known exactly and can be mapped to that of an ideal Fermi gas [36]. We call this limit full fermionization. Note that for a system of two A atoms and one B atom, the order in which the limits are taken (i.e., if one first takes

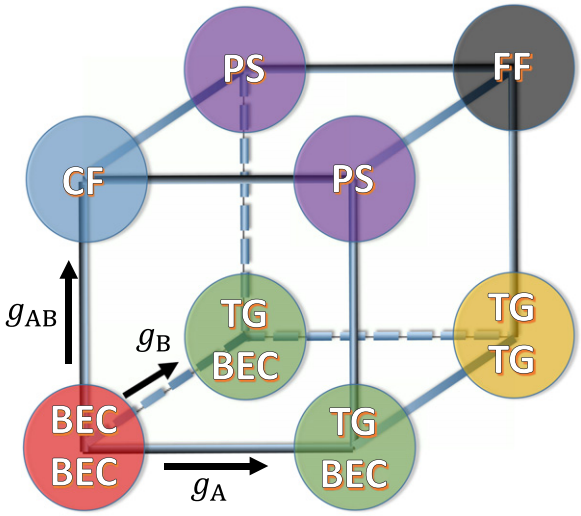

Figure 1. Schematic of all regimes in the few-atom limit. The following abbreviations are used. BEC: Bose–Einstein condensate; TG: Tonks–Girardeau gas; CP: composite fermionization; PS: phase separation; FF: full fermionization.

$g_A \to \infty$ and then $g_{AB} \to \infty$ or v.v.) determines the particular ground state that is reached [38]. In the following we will calculate and discuss the complete phase diagram, which includes the transitions between these limits. To restrict the large number of free parameters, we note that the transition between TG and the phase separation limit is symmetric when switching the values of g_A and g_B, and we can therefore circumscribe the discussion to the situation where g_B vanishes, and change g_A. In the following, we will use harmonic oscillator units and scale all lengths in units of oscillator length $a_0 = \sqrt{\hbar/(m\omega)}$ and all energies in units of level spacing $\hbar\omega$.

To solve the Hamiltonian (1), we use two different numerical approaches: direct diagonalization [42] and DMC [69]. The former allows us to calculate the full density matrix of the system and therefore gives us access to all single- and multi-particle correlations. However, since it is limited to small particle numbers, the latter will be used to check for trends when the number of particles becomes larger. While DMC is well described in the literature, let us briefly explain our approach to direct diagonalization. For this we expand the second quantized field operators into eigenfunctions $\phi_n(x)$ of the single-particle (SP) Hamiltonian for the harmonic oscillator:

$$\hat{\psi}_A(x) = \sum_{n=1}^{n_A} \hat{a}_n \phi_n(x), \qquad \text{and} \qquad \hat{\psi}_B(x) = \sum_{n=1}^{n_B} \hat{b}_n \phi_n(x), \tag{2}$$

where the creation and annihilation operators $\hat{a}_k^\dagger$ and $\hat{a}_k$ satisfy the bosonic commutation relations $[\hat{a}_k, \hat{a}_l^\dagger] = \delta_{kl}$, $[\hat{a}_k, \hat{a}_l] = [\hat{a}_k^\dagger, \hat{a}_l^\dagger] = 0$ and similarly for $\hat{b}_k^\dagger$ and $\hat{b}_k$, while all commutators between operators belonging to different species vanish. Here, $n_{A(B)}$ is the number of modes used in the expansion. The Hamiltonian can then be written as [46]:

$$\hat{H}_A = \sum_k \hat{a}_k^\dagger \hat{a}_k \hbar\omega \left(\frac{1}{2} + k\right) + \frac{1}{2} \sum_{klmn} \hat{a}_k^\dagger \hat{a}_l^\dagger \hat{a}_m \hat{a}_n V_{klmn}^A \tag{3}$$

$$\hat{H}_{\mathrm{B}} = \sum_{k} \hat{b}_k^{\dagger} \hat{b}_k \hbar\omega \left(\frac{1}{2} + k \right) + \frac{1}{2} \sum_{klmn} \hat{b}_k^{\dagger} \hat{b}_l^{\dagger} \hat{b}_m \hat{b}_n V_{klmn}^{\mathrm{B}} \tag{4}$$

$$\hat{H}_{\mathrm{int}} = \sum_{klmn} \hat{a}_k^{\dagger} \hat{b}_l^{\dagger} \hat{b}_m \hat{a}_n V_{klmn}^{\mathrm{AB}} , \tag{5}$$

where:

$$V_{klmn}^{\mathrm{A(B)}} = g_{\mathrm{A(B)}} \int \mathrm{d}x \; \phi_k^*(x) \phi_l^*(x) \phi_m(x) \phi_n(x), \tag{6}$$

$$V_{klmn}^{\mathrm{AB}} = g_{\mathrm{AB}} \int \mathrm{d}x \; \phi_k^*(x) \phi_l^*(x) \phi_m(x) \phi_n(x). \tag{7}$$

The ground state can be expressed in terms of Fock vectors $\Psi_0 = \sum_{i=1}^{\Omega} c_i \Phi_i$ with:

$$\Phi_i = D_i^{\mathrm{A}} D_i^{\mathrm{B}} \left(\hat{a}_1^{\dagger} \right)^{N_{1,i}^{\mathrm{A}}} \ldots \left(\hat{a}_{n_{\mathrm{A}}}^{\dagger} \right)^{N_{n_{\mathrm{A}},i}^{\mathrm{A}}} \left(\hat{b}_1^{\dagger} \right)^{N_{1,i}^{\mathrm{B}}} \ldots \left(\hat{b}_{n_{\mathrm{B}}}^{\dagger} \right)^{N_{n_{\mathrm{B}},i}^{\mathrm{B}}} \Phi_0, \tag{8}$$

where $D_i^{\mathrm{A(B)}} = \left(N_{1,i}^{\mathrm{A(B)}}! \ldots N_{n_{\mathrm{A(B)}},i}^{\mathrm{A(B)}}! \right)^{-\frac{1}{2}}$, and Φ_0 is the vacuum. The occupation numbers of the n_{A} (n_{B}) modes for each component are given by $N_{1,i}^{\mathrm{A}}, \ldots, N_{n_{\mathrm{A}},i}^{\mathrm{A}}$ ($N_{1,i}^{\mathrm{B}}, \ldots, N_{n_{\mathrm{B}},i}^{\mathrm{B}}$). The dimension of the Hilbert space is $\Omega = \Omega_{\mathrm{A}} \Omega_{\mathrm{B}}$ with $\Omega_{\mathrm{A(B)}} = (N_{\mathrm{A(B)}} + n_{\mathrm{A(B)}} - 1)!/[N_{\mathrm{A(B)}}!(n_{\mathrm{A(B)}} - 1)!]$. Note that Ω increases exponentially with the number of particles and modes, which is the reason why the numerical solution using this approach is restricted to a small number of atoms.

A good ansatz for the unnormalized ground-state wavefunction of the mixture, when $g_{\mathrm{B}} = 0$ and outside of the phase-separated regime, can be constructed using the solution for non-interacting atoms in the harmonic trap $\Phi(X) = \exp[-\sum x_i^2/2]$, $X = \{x_i\}$ and $Y = \{y_i\}$, as in [46]:

$$\Psi(X, Y) = \Phi(X) \, \Phi(Y) \prod_{j<k}^{N_{\mathrm{A}}} \left| x_k - x_j - a_{\mathrm{A}} \right| \prod_{k}^{N_{\mathrm{A}}} \prod_{j}^{N_{\mathrm{B}}} \left| x_k - y_j - a_{\mathrm{AB}} \right|. \tag{9}$$

Here the 1D *s*-wave scattering length a_{A} for the intra-species interactions and a_{AB} for the inter-species interactions are related to the 1D coupling constants as $g_{\mathrm{A}} = -2\hbar^2/(m a_{\mathrm{A}})$ and $g_{\mathrm{AB}} = -2\hbar^2/(m a_{\mathrm{AB}})$, and we assume that both coupling constants are non-negative, corresponding to repulsive interactions. For practical purposes, we find that the coupling constant $g = 20$ is close enough to the infinite limit, and therefore we use this value in the direct diagonalization method for describing the large coupling constant limits.

3. Balanced mixtures

In the following, we will first concentrate on systems in which both components have the same particle number. Unless otherwise stated, we will use $N_{\mathrm{A}} = N_{\mathrm{B}} = 2$.

3.1. Densities

The main feature of the density evolution in this system is the occurrence of phase separation for increasing inter-species interactions. However, this process takes two, fundamentally different, forms: in the composite fermionization limit, atoms of different species avoid each

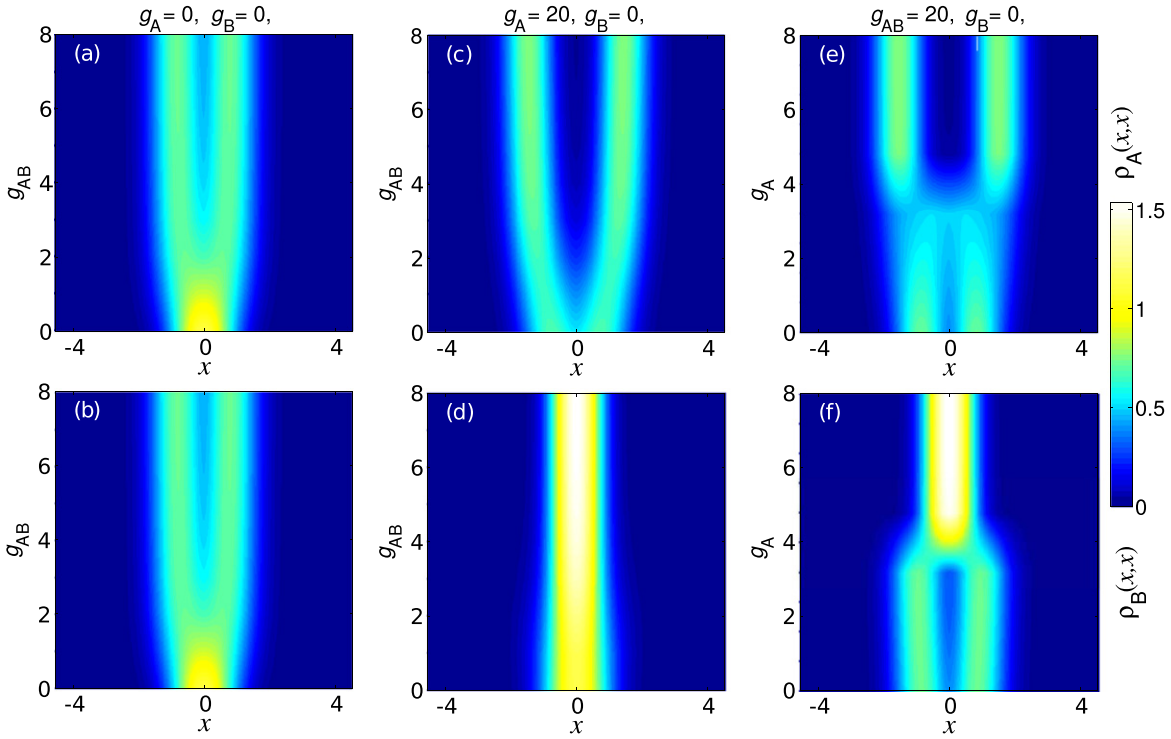

Figure 2. Upper (lower) row shows the density of the A (B) species, for $N_A = N_B = 2$. Panels (a–d) show the evolution for increasing g_{AB}, starting from the BEC–BEC limit (panels (a) and (b), $g_A = g_B = 0$) or the TG–BEC limit (panels (c) and (d), $g_A = 20$, $g_B = 0$). Panels (e) and (f) display the transition between the composite fermionization and the phase-separated limits [$g_B = 0$, $g_{AB} = 20$].

other, even though the species' densities still occupy the same space, whereas in the phase separation limit the overlap of the respective densities goes to zero.

The density along the transition from the BEC–BEC limit (all couplings small) to the composite fermionization limit (g_{AB} large) is shown in figures 2(a) and (b). There are crucial differences in the evolution of the density along the transition from the TG–BEC to the phase separation limit (figures 2(c) and (d)). One immediately notices that the transition into the composite fermionization state happens at a finite value of $g_{AB} \sim 2$, whereas the transition to the phase-separated regime happens already for very small values of g_{AB}. Also, the final states reached in the composite fermionization or the phase separation limit are very different.

This difference in the final states can be understood by looking at the one-body density matrix (OBDM) given by:

$$\rho_1^{\mathrm{A}}(x, x') = N_{\mathrm{A}} \int \mathrm{d}x_2 \cdots \mathrm{d}x_{N_{\mathrm{A}}}\, \mathrm{d}y_1 \cdots \mathrm{d}y_{N_{\mathrm{B}}}\, |\Psi|^2 \tag{10}$$

$$= \sum\nolimits_k f_k(x) f_k(x') \lambda_{\mathrm{A}}^k \tag{11}$$

with a similar expression for $\rho_1^{\mathrm{B}}(x, x')$. The decomposition in terms of natural orbitals $f_k(x)$ of the OBDM and their corresponding occupations λ_{A}^k is given in equation (11). The densities shown in figure 2 are the diagonals of these matrices, calculated with direct diagonalization. As

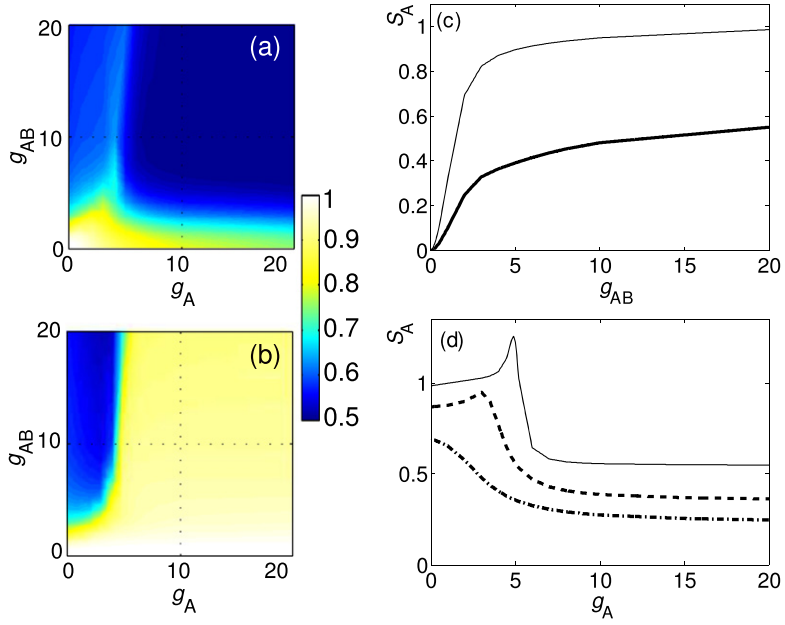

Figure 3. Largest occupation numbers of the natural orbitals for (a) the A species, λ_0^{A}, and (b) the B species, λ_0^{B}. (c) von Neumann entropy for $N_{\mathrm{A}} = N_{\mathrm{B}} = 2$ as a function of g_{AB} for $g_{\mathrm{A}} = 0$ (thick line) and $g_{\mathrm{A}} \to \infty$ (thin line). (d) von Neumann entropy as a function of g_{A} for the cases $g_{\mathrm{AB}} = 2, 4, 20$ (dash-dotted, dashed, and solid line, respectively) for $N_{\mathrm{A}} = N_{\mathrm{B}} = 2$.

discussed in reference [46], the OBDMs of both components in the composite fermionization limit are identical and show two peaks. Conversely, in the phase separation limit, the OBDM of B shows a single peak located at the center of the trap, while the OBDM for A shows two peaks at the edges. The largest used value of the coupling constant $g = 8$ is large enough so that the density profiles shown in figure 2 are practically the same as for the infinite coupling constant.

Finally, the transition from the composite fermionization to the phase-separated regime is shown in figures 2(e) and (f). One can see that the spatial separation of the clouds happens for a finite value of g_{A}. At the transition between both limits, the OBDMs of both species show a complicated structure, which we discuss in detail in subsection 3.4.

3.2. Coherence and entanglement

Since increasing the coupling constant will drive the system from the weakly to the strongly correlated regime, the coherence is a good quantity for identifying different regions in the phase diagram. It can be characterised by the largest eigenvalue of the OBDMs (11), $\lambda_0^{\mathrm{A(B)}}$, which provides the largest occupation of a natural orbital. In our numerical calculations with direct diagonalization, we normalize the OBDM to 1 instead of the number of atoms. In figures 3(a) and (b) we show the largest occupation numbers for the A and the B species, respectively, over the whole range of interactions. Note that all eigenvalues of each component sum up to 1, in accordance with the chosen normalization.

One can see from figure 3(a) that the coherence in the A species decreases monotonically along the transition from the BEC–BEC ($\lambda_0^{\mathrm{A}} = 1$) to the TG–BEC ($\lambda_0^{\mathrm{A}} \sim 0.7$) limit, as well as to the composite fermionization limit ($\lambda_0^{\mathrm{A}} \sim 0.55$). However, the transition for increasing g_{A} at a finite g_{AB} shows that a maximum of coherence is reached for finite values of $g_{\mathrm{A}} \sim 5$, which corresponds roughly to the value where the cloud de-mixing happens (see figures 2(e) and (f)). This maximum in coherence within species A is very surprising, as usually the presence of interactions is thought of as detrimental to coherence. Here, however the presence of interactions within the A component to a certain degree 'counterbalance' the interactions between the species and therefore allows us to re-establish a higher degree of coherence again. Note that after the de-mixing transition, the coherence within species A goes down again, which is a clear indication that the enhancement is somehow mediated using the overlap with species B.

As expected, species B shows a large degree of coherence in all limits, except the composite fermionization one (see figure 3(b)). However, the re-establishment of coherence along the transition from composite fermionization to the phase-separated limit happens over a definite and narrow region, which corresponds to the area in which the coherence in species A shows a maximum.

One might at this point wonder how the transition to phase separation manifests itself during the transition from the TG–BEC to the phase-separated limit, as no obvious signature is visible in the coherence phase diagram. The answer is that phase separation happens already for small values of g_{AB}, which can be seen in figure 2(c).

It is important to observe that there are no phase transitions in the whole phase diagram. The ground-state energy is always a continuous and smooth function of the parameters so that the transition between the different regimes is of a crossover type.

Closely related to the coherence in the sample is the entanglement between the two components. This can be quantified by calculating the von Neumann entropy, $S_{\mathrm{A}} = -\mathrm{Tr}\left(\rho_{\mathrm{A}} \ln \rho_{\mathrm{A}}\right)$, which is a function of the reduced density matrix for a single component:

$$\rho_{\mathrm{A}} = \mathrm{Tr}_{\mathrm{B}}\rho = \sum_i \left\langle \Phi_i^{\mathrm{B}} \left| \Psi_0 \right\rangle \left\langle \Psi_0 \right| \Phi_i^{\mathrm{B}} \right\rangle. \tag{12}$$

Here $\rho = |\Psi_0\rangle\langle\Psi_0|$ is the density matrix, Ψ_0 is the system ground state, and:

$$\Phi_i^{\mathrm{B}} = D_i^{\mathrm{B}} \left(\hat{b}_1^{\dagger}\right)^{N_{1,i}^{\mathrm{B}}} \ldots \left(\hat{b}_{n_{\mathrm{B}}}^{\dagger}\right)^{N_{n_{\mathrm{B}},i}^{\mathrm{B}}} \Phi_0 \tag{13}$$

is the Fock vector for species B only. This matrix is obtained by means of direct diagonalization. In figure 3(c) we show the von Neumann entropy S_{A} along the transition between BEC–BEC and composite fermionization. S_{A} can be seen to approach a constant value as g_{AB} is increased, corresponding to the large inter-species correlations present in the composite fermionization. The same plot also shows S_{A} along the transition between TG–BEC and the phase-separated limit. The two species are less correlated throughout this transition, but still S_{A} saturates to a constant value in the phase-separated limit. In figure 3(d) we plot S_{A} for different values of g_{AB} when g_{A} is tuned from zero to a large value. When $g_{\mathrm{AB}} = 20$, this corresponds to the transition between composite fermionization and a phase-separated gas. We observe a peak which coincides with the crossover between both limits. This peak disappears as g_{AB} is reduced, as observed in the curves for $g_{\mathrm{AB}} = 4, 2$ in figure 3(d). For $g_{\mathrm{AB}} = 0$, S_{A} is zero for every value of g_{A}.

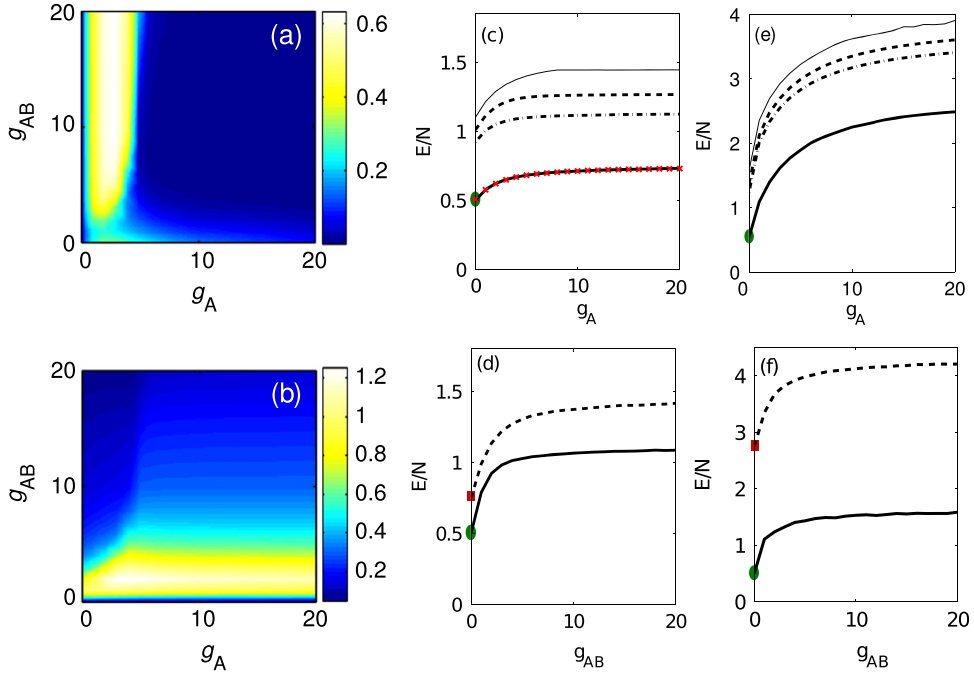

Figure 4. Panel (a) shows the average interaction energy of species A, $\langle U_A \rangle$, and panel (b) the average interaction energy between species A and B, $\langle U_{AB} \rangle$. Here $N_A = N_B = 2$, and $g_B = 0$. Panel (c) reports the energy per atom as a function of g_A for $g_{AB} = 0$, 2, 4, 20 (thick solid, dash-dotted, dashed, and thin solid lines, respectively) for $N_A = N_B = 2$. The red crosses overlapping with the black thick line represent the analytical result [53]. (d) Energy per atom as a function of g_{AB} for $g_A = 0$ (solid line) and $g_A \to \infty$ (dashed line), for $N_A = N_B = 2$. Panels (e) and (f) represent the energy per atom for $N_A = N_B = 10$, with the same layout as figures (c) and (d), respectively. In panels (c)–(f), the green circles indicate the energy in the BEC–BEC limit. In panels (d) and (f), the red squares indicate the energy in the TG–BEC limit.

3.3. Interaction energies

An interesting question is how the interaction energy changes across the transitions between the different limits. The average interaction energy in species A is:

$$\langle U_A \rangle = \left\langle \frac{1}{2} \sum_{klmn} \hat{a}_k^\dagger \hat{a}_l^\dagger \hat{a}_m \hat{a}_n V_{klmn}^A \right\rangle. \tag{14}$$

We display this energy in figure 4(a). For zero g_A there are no interactions between A atoms, and $\langle U_A \rangle$ is equal to zero. By increasing g_A, the energy $\langle U_A \rangle$ first grows as correlations are being introduced. For larger repulsion, particles avoid each other, which leads to very strong correlations, and the interaction energy drops down to zero. Starting from the BEC–BEC region, this is a long process, however; for a finite value of g_{AB} this happens over a very well defined domain of the parameter g_A, located at small values of g_A. Note that for $g_A = 0$ and in the presence of interaction with species B, the particles in species A are much more localized than for $g_{AB} = 0$. Therefore, small increases in the interaction strength g_A lead to strong

increases in the interaction energy $\langle U_{\rm A}\rangle$. This is also consistent with the maximum found in the correlation strength within component A.

The interaction energy goes to zero in the TG–BEC limit, which is the behaviour expected for a single component gas [30–33], as the increased energy is now stored in the single particle harmonic oscillator energies. During the whole process the total energy is increased from:

$$E_{\rm BECBEC} = \frac{1}{2}\left(N_{\rm A} + N_{\rm B}\right) \tag{15}$$

to

$$E_{\rm TGBEC} = \frac{1}{2}\left(N_{\rm B} + N_{\rm A}^2\right). \tag{16}$$

The energy for $N_{\rm A} = N_{\rm B} = 2$ is shown in figure 4(c). The energy obtained by the direct diagonalization and DMC methods coincides. For no interactions between different species, $g_{\rm AB} = 0$, and the energy can be expressed as $E = \hbar\omega + E_2(g_{\rm A})$, where $E_2(g_{\rm A})$ is the energy of two trapped particles interacting with the coupling constant $g_{\rm A}$ [53]. In order to prove that the described limits exist in larger systems, we calculate the energy for $N_{\rm A} = N_{\rm B} = 10$ particles with the DMC method.

The energy per particle in the BEC–BEC limit (15) does not depend on the number of particles, $E_{\rm BECBEC}/N = 1/2$. We show this in figures 4(c) and (e), with green circles for $N_A = N_B = 2$ and 10.

In figures 4(d) and (f), we depict the energy per particle as a function of $g_{\rm AB}$, starting from the BEC–BEC (solid line) and the TG–BEC (dashed line) limits. Here the green circles (red squares) indicate the energy per atom in the BEC–BEC (TG–BEC) limit. The energy in the TG–BEC limit given by equation (16) is $E_{\rm TGBEC}/N = 3/4$ for $N_{\rm A} = N_{\rm B} = 2$ and $E_{\rm TGBEC}/N = 11/4$ for $N_{\rm A} = N_{\rm B} = 10$. In the transition from the BEC–BEC limit to the composite fermionization one, the energy saturates to a certain value for which we do not have an analytical prediction. Also, a monotonic behavior is observed in the transition from the TG–BEC to the phase separation limit (figures 4(d) and (f)).

The average interaction energy between both species, given by:

$$\left\langle U_{\rm AB}\right\rangle = \left\langle \sum_{klmn} \hat{a}_k^\dagger \hat{b}_l^\dagger \hat{b}_m \hat{a}_n V_{klmn}^{\rm AB} \right\rangle, \tag{17}$$

is important to quantify the transition to the composite fermionization or the phase-separated regime. The interaction energy rapidly increases from zero to a maximum at $g_{\rm AB} \approx 2$ (see figure 4(b)) and decreases again toward zero for $g_{\rm AB} \to \infty$. For $g_{\rm A} = 0$, this corresponds to building up strong correlations between the particles of different species in the composite fermionization limit, whereas in the limit of large $g_{\rm A}$, this reflects the transition to a *macroscopic* phase separation of the two components.

3.4. Correlation matrices

Since in the presence of strong interactions the system has non-trivial many-body correlations, it is interesting to look not only at single-particle densities, but also at pair-wise correlation functions. The single-particle densities are quantified by the OBDM (equation (10)). For particles of the same species, the two-particle correlations are quantified by the two-body

distribution function (TBDF):

$$\rho_2^{\mathrm{A}}(x_1, x_2) = N_{\mathrm{A}}\left(N_{\mathrm{A}} - 1\right) \int \mathrm{d}x_3 \cdots \mathrm{d}x_{N_{\mathrm{A}}} \mathrm{d}y_1 \cdots \mathrm{d}y_{N_{\mathrm{B}}} \ |\Psi|^2, \tag{18}$$

with an analogous expression for B. If the two atoms stem from different species, their pair-wise correlations are captured in the cross two-body distribution function (CTBDF) given by:

$$\rho_2^{\mathrm{AB}}(x_1, y_1) = N_{\mathrm{A}}\ N_{\mathrm{B}} \int \mathrm{d}x_2 \cdots \mathrm{d}x_{N_{\mathrm{A}}} \mathrm{d}y_2 \cdots \mathrm{d}y_{N_{\mathrm{B}}} \ |\Psi|^2. \tag{19}$$

Both functions are proportional to the joint probability for finding two atoms at two given positions.

It was shown in [43, 46] that the correlation functions are very useful for a description of the composite fermionization and the phase separation limits. In the following, we will carefully look at the transition between these two limits. The phase separation occurs for g_{A} and g_{AB} large and implies a density distribution with atoms of species B localized at the center of the trap, while the atoms of species A gather at the edges of the density of B. As discussed above, the de-mixing point can also be identified in the coherence, the interaction energies, and the entanglement.

In figure 5 we show the OBDMs, TBDFs and CTBDFs just before ($g_{\mathrm{A}} = 5$) and just after ($g_{\mathrm{A}} = 7$), the crossover. The upper and lower rows show numerical results, while the middle row represents the analytical results obtained from ansatz (9) with $a_{\mathrm{A}} = a_{\mathrm{AB}} = 0$. One can see that just before the crossover, the densities of both species, i.e., the diagonals of the OBDMs, significantly overlap (panels (a) and (b)), whereas the overlapping is greatly reduced after the crossover (panels (k) and (l)). The TBDFs and CTBDFs before and after the crossover (panels (c)–(e) and (m)–(o), respectively) demonstrate that the atoms of species A are anticorrelated with themselves and with the atoms of species B, as both functions vanish along the diagonal. Note that at the same time, atoms of species B are not strongly correlated. This is also captured by ansatz (9), where strong correlations are induced by zeros whenever A-A or A-B atoms overlap (see panels (f)–(j)). All densities and pair correlations computed with this ansatz qualitatively resemble the exact correlation functions just before demixing. However, the ansatz fails to describe the ground state of the system once it has phase separated.

Let us note that the TBDF for the A species shown in figure 5(c) corresponding to the crossover for $N_{\mathrm{A}} = N_{\mathrm{B}} = 2$ looks similar to those obtained for $N_{\mathrm{A}} = 4$ and a very heavy atom in component B (discussed in [56, 57]) or a large number of atoms in B (discussed in [42]). Those cases belong to the phase-separated limit, in which B formed a material barrier. Therefore, the two atoms of A stay at each side of B. Very differently in this case, there are only two atoms of A, and they can be localized in either side of B.

For $N_{\mathrm{A}} = N_{\mathrm{B}} > 2$, the results discussed above remain qualitatively valid. We show in figure 6(a) the densities for the composite fermionization limit when $N_{\mathrm{A}} = N_{\mathrm{B}} = 2, 4, 6, 8, 10$ calculated with DMC. In this situation, the OBDMs are equal for both species. The two peaks present in the density tend to spatially separate as N is increased as a consequence of the large repulsion between both species, which increases with the number of atoms. In figures 6(b) and (c), we show the densities for B and A, respectively, in the phase-separated limit. As N is increased, the atoms of B have a greater tendency to localize in the center of the trap. The numerically calculated density for A shows that this component is localized at each side of B, forming two TG gases with $N/2$ atoms in each side. Note that this is reminiscent of effects in two-component fermionic systems [71], where it was recently shown that a single-particle

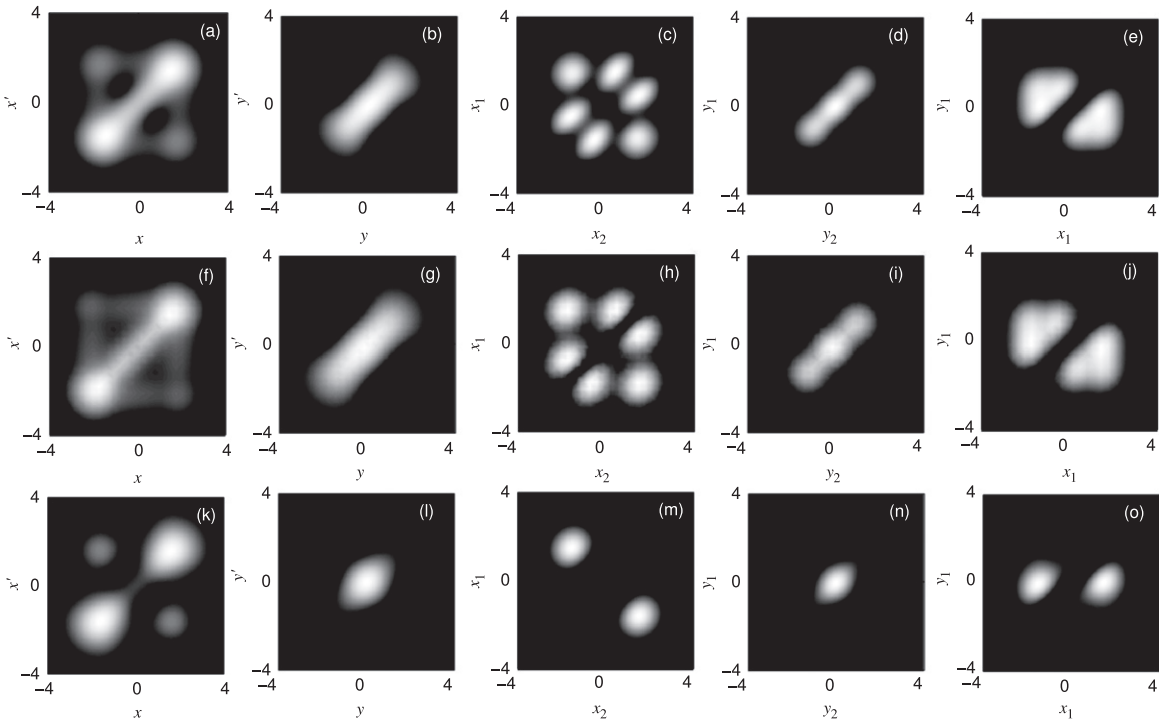

Figure 5. The first and second columns show the OBDMs; the third and fourth columns the TBDFs, each time for species A and B, respectively; and the last column shows the CTBDF. g_{AB} is large in all panels. The first and last row display the numerical result obtained for a value of g_A just before and after the crossover, respectively, and the middle row shows the results obtained from calculating the OBDMs and TBDF directly using the ansatz given in equation (9) with $a_A = a_{AB} = 0$. Good agreement is clearly visible with the numerical results before the crossover.

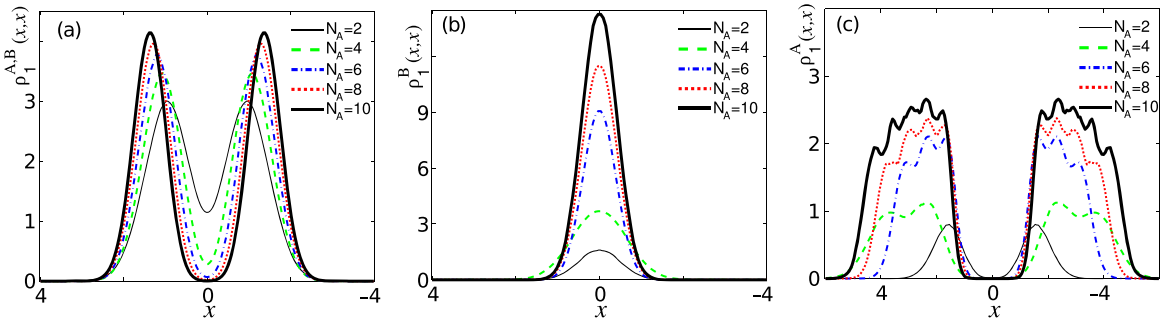

Figure 6. Densities with $N_A = N_B = 2, 4, 6, 8, 10$ atoms. (a) Densities plotted in the composite fermionization limit, showing that the two peaks appear farther appart as N is increased. (b) Densities for B in the phase-separated limit. The atoms tend to localize more and more in the center as N is increased. (c) Densities for A in the phase-separated limit. The atoms of A are in the edges of B, forming two TG gases with $N/2$ atoms.

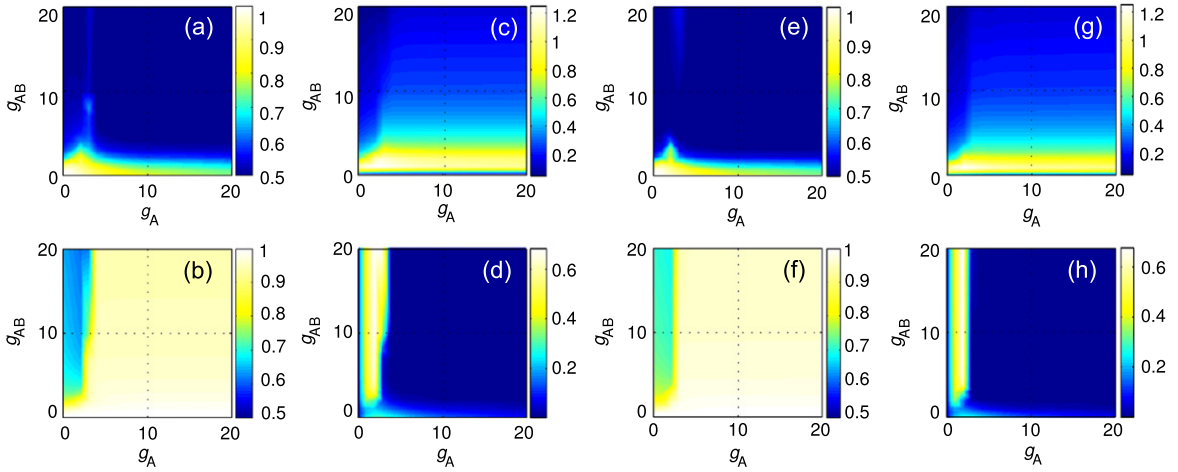

Figure 7. Largest occupations λ_0^A and λ_0^B of a natural orbital and average interaction energies as a function of g_A and g_{AB}, when $N_A = 2$, $g_B = 0$. (a) and (b) show λ_0^A and λ_0^B when $N_B = 3$. (c) and (d) represent $\langle U_A \rangle$ and $\langle U_{AB} \rangle$, respectively, for the same case. (e)–(h) represent the same when $N_B = 4$. The region in which B is not condensed is reduced as N_B is increased, keeping N_A constant.

minority component will be trapped in the center of the majority component due to correlations in the wave function.

The difference in the energy between BEC–BEC and TG–BEC regimes is further increased in balanced systems of a larger size, $N_A = N_B \gg 1$. Indeed, according to equation (15), the energy in the BEC–BEC scales linearly with the number of particles N, which is a typical behavior of weakly interacting bosons. Instead, in the TG–BEC limit, according to equation (16) the dependence on N is quadratic. This resembles the behavior of the energy of fermionic particles and is a manifestation of Girardeau mapping. Comparing the results for $N_A = N_B = 2$ with $N_A = N_B = 10$, we already observe how the difference in the energy between limits increases (see figure 4).

4. Effect of a larger population in the weakly interacting species

In the imbalanced case $N_B > N_A$, the wavefunction (9) can be equally used as an ansatz for the exact ground state of the systems. The four limits discussed above equally exist. Nevertheless, the weakly interacting species now has a greater tendency to localize in the center of the trap and condense, which modifies the boundaries between the different regimes associated to these limits. In figures 7(a)–(b) and (e)–(f) we report the largest eigenvalue of the OBDM for species A and B to quantify the coherence, covering the whole range of coupling constants, when $N_A = 2$ and $N_B = 3$, 4, respectively. As N_B is increased we observe that the region in which B is not condensed is reduced (the light blue area in figures 7(b) and (f)). Moreover, the minimum value of λ_0^B, which occurs in this non-condensed area, grows with N_B for fixed N_A. Notice also that the area in which λ_0^A approaches the largest possible value $\lambda_0 = 1$, i.e., close to the g_A axis, is reduced as N_B is increased.

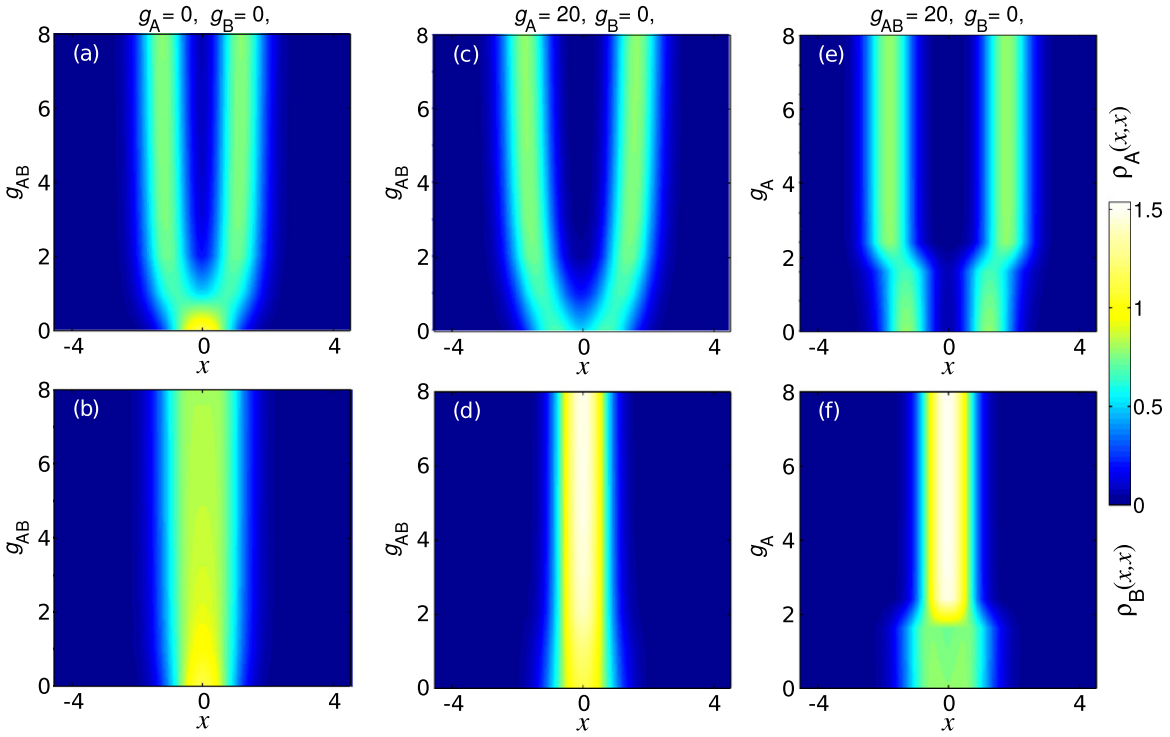

Figure 8. Densities for both species between the four different regimes. Upper (lower) row is the density for A (B) species, when $N_A = 2$ and $N_B = 4$. Panel layout is as in figure 2. The density for B in the composite fermionization limit is more similar to the one obtained in the phase separation limit.

In figures 8(a) and (b), we show the density profiles for A and B along the transition between the BEC–BEC limit and composite fermionization for $N_A = 2$ and $N_B = 4$. The atoms of species B are now more concentrated in the center than when both populations were equal, even though species B is still not fully condensed. The two peaks in species A appear at a smaller value of g_{AB} and are more spatially separated than in the case $N_B = N_A$. We note that in the composite fermionization limit, the density of species A in the center for the balanced case is finite, while in the imbalanced case it vanishes (compare figures 2(a) and 8(a)). The density profiles along the transition between the TG–BEC and the phase-separated gas are presented in figures 8(c) and (d). Comparing with the balanced case plotted in figures 2(c) and (d), we notice that, in the phase separation limit, the two peaks in the density profile of A are now more separated, and the squeezing in the density of B is smaller. The average interaction energy $\langle U_{AB} \rangle$ (figures 7(c) and (g)) tends to zero when phase separation occurs. Figures 8(e) and (f) report the density along the transition between composite fermionization and phase separation. We observe that the position of the two peaks in the density profile of A in the phase-separated, and the composite fermionization limit is closer than in the balanced case (compare with figures 2(e) and (f)). Also, the crossover occurs now at a smaller value of g_A. The average interaction energy $\langle U_A \rangle$ (figures 7(d) and (h)) decreases abruptly to zero after the crossover. We conclude that for larger imbalances, $N_B \gg N_A$, the composite fermionization region is highly suppressed, and, therefore, the surviving limits are those associated to BEC–BEC, TG–BEC, and the phase-separated mixtures.

If the macroscopic limit is reached in such a way that the number of atoms in one of the species is fixed, the minority species plays the role of an impurity that perturbs the majority species. The relative contribution of the minority species to the energy becomes smaller, and a polaronic description might be applicable.

5. Summary and conclusions

Current experimental advances in ultracold atomic physics allow one to scrutinize the onset and evolution of correlations in few-atom bosonic fluids. Small samples can be trapped, and their interactions can be largely tuned, thus providing a fantastic ground to understand how quantum many-body correlations build up in small samples. Binary mixtures are specially appealing, as they provide the first step toward understanding the effect of environments on quantum systems in a controlled way. To advance in that direction, we study the effect of embedding a quantum fluid (component A) within a second quantum fluid (B) with tunable intra- and inter-species interactions at zero temperature. We fix the coupling constant of B-B interactions to that of ideal bosons, $g_B = 0$, and vary A-A and A-B interactions in a wide range, $0 \leqslant g_A < \infty$, $0 \leqslant g_{AB} < \infty$. This permits us to explore the phase diagram for a variety of regimes. The energy, one- and two-body correlation functions, density profiles, and von Neumann entropy are calculated exactly, using the diagonalization method. For larger system sizes, the results are complemented with the energy and density profiles obtained by the diffusion Monte Carlo method.

We have described the transition between the following four limits: (a) the BEC–BEC limit, where both components interact weakly and thus remain condensed, (b) the BEC–TG limit, where the two components interact weakly among each other and A has strong intra-species interaction, (c) the composite fermionization limit, where the interaction between both species is large, inducing strong correlations within both species, and (d) a phase separation limit, where both the intra-species interaction in A and the inter-species interactions are large. We show that the transition between the different limits involves sophisticated changes in the one- and two-body correlations. The energetic properties change in a smooth way, with the energy and its derivatives remaining continuous, which implies a transition of a crossover type rather than a true phase transition. At the same time, the entanglement between the two components has a much sharper dependence on the interactions. This is demonstrated by reporting the von Neumann entropy, which manifests a sharp peak along the transition between composite fermionization and phase separation. The evolution of the density profiles of A and B components is studied in detail both for the balanced and the imbalanced case. The effect of a large number of particles on the energy and the density profiles is discussed. We analyze the coherence properties by expanding the one-body density matrix in natural orbitals and obtaining the occupation numbers. We demonstrate that full condensation (largest occupation number equal to one) for A species is reached only in the BEC–BEC regime, while the weakly interacting B species also remains fully condensed in the TG–BEC regime, and the condensation is almost complete in the phase separation regime. We argue that the described picture of the transition between four mentioned regimes remains valid also in macroscopically large balanced mixtures, $N_A = N_B \to \infty$. Conversely, when the macroscopic limit is reached by increasing the number of atoms of the weakly-interacting species $N_B \to \infty$, the composite fermionization limit is suppressed. Therefore the phase diagram in this highly imbalanced case

resembles that expected within a mean-field approach. The studied effects are relevant to ongoing and future experiments with small two-component systems.

Acknowledgements

This project was supported by Science Foundation Ireland under Project No. 10/IN.1/I2979. We acknowledge also partial financial support from the DGI (Spain) Grants No. FIS2011–25275, FIS2011–24154, and the Generalitat de Catalunya Grant No. 2009SGR-1003. GEA and BJD are supported by the Ramón y Cajal program, MEC (Spain).

References

[1] Myatt C J, Burt E A, Ghrist R W, Cornell E A and Wieman C E 1997 *Phys. Rev. Lett* **78** 586
[2] Stamper-Kurn D M, Andrews M R, Chikkatur A P, Inouye S, Miesner H-J, Stenger J and Ketterle W 1998 *Phys. Rev. Lett.* **80** 2027
[3] Hall D S, Matthews M R, Ensher J R, Wieman C E and Cornell E A 1998 *Phys. Rev. Lett.* **81** 1539
[4] Catani J, DeSarlo L, Barontini G, Minardi F and Inguscio M 2008 *Phys. Rev.* A **77** 011603(R)
[5] McCarron D J, Cho H W, Jenkin D L, Koppinger M P and Cornish S L 2011 *Phys. Rev.* A **84** 011603(R)
[6] Ho T-L and Shenoy V B 1996 *Phys. Rev. Lett.* **77** 3276
[7] Law C K, Pu H, Bigelow N P and Eberly J H 1997 *Phys. Rev. Lett.* **79** 3105
[8] Esry B D, Greene C H, Burke J P and Bohn J L 1997 *Phys. Rev. Lett.* **78** 3594
[9] Timmermans E 1998 *Phys. Rev. Lett.* **81** 5718
[10] Pu H and Bigelow N P 1998 *Phys. Rev. Lett.* **80** 1130
[11] Goldstein E V and Meystre P 1997 *Phys. Rev.* A **55** 2935
[12] Busch Th, Cirac J I, Perez-Garcia V M and Zoller P 1997 *Phys. Rev.* A **56** 2978
[13] Ao P and Chui S T 1998 *Phys. Rev.* A **58** 4836
[14] Trippenbach M, Goral K, Rzazewski K, Malomed B and Band Y B 2000 *J. Phys. B: At. Mol. Opt. Phys.* **33** 4017
[15] Cazalilla M A and Ho A F 2003 *Phys. Rev. Lett.* **91** 150403
[16] Alon O E, Streltsov A I and Cederbaum L S 2006 *Phys. Rev. Lett.* **97** 230403
[17] Mishra T, Pai R V and Das B P 2007 *Phys. Rev.* A **76** 013604
[18] Kleine A, Kollath C, McCulloch I P, Giamarchi T and Schollwock U 2008 *Phys. Rev.* A **77** 013607
[19] Ho T-L 1998 *Phys. Rev. Lett.* **81** 742
[20] Ohmi T and Machida K 1998 *J. Phys. Soc. Japan* **67** 1822
[21] Eisenberg E and Lieb E H 2002 *Phys. Rev. Lett.* **89** 220403
[22] Fuchs J N, Gangardt D M, Keilmann T and Shlyapnikov G V 2005 *Phys. Rev. Lett.* **95** 150402
[23] Guan X-W, Batchelor M T and Takahashi M 2007 *Phys. Rev.* A **76** 043617
[24] Lewandowski H J, Harber D M, Whitaker D L and Cornell E A 2002 *Phys. Rev. Lett.* **88** 070403
[25] McGuirk J M, Lewandowski H J, Harber D M, Nikuni T, Williams J E and Cornell E A 2002 *Phys. Rev. Lett.* **89** 090402
[26] McGuirk J M, Harber D M, Lewandowski H J and Cornell E A 2003 *Phys. Rev. Lett.* **91** 150402
[27] Girardeau M 1960 *J. Math. Phys.* **1** 516
[28] Girardeau M D, Wright E M and Triscari J M 2001 *Phys. Rev.* A **63** 033601
[29] Gangardt D M and Shlyapnikov G V 2003 *Phys. Rev. Lett.* **90** 010401
[30] Alon O E and Cederbaum L S 2005 *Phys. Rev. Lett.* **95** 140402
[31] Deuretzbacher F, Bongs K, Sengstock K and Pfannkuche D 2007 *Phys. Rev.* A **75** 013614
[32] Ernst T, Hallwood D W, Gulliksen J, Meyer H-D and Brand J 2011 *Phys. Rev.* A **84** 023623
[33] Brouzos I and Schmelcher P 2012 *Phys. Rev. Lett.* **108** 045301

[34] Paredes B, Widera A, Murg V, Mandel O, Folling S, Cirac I, Shlyapnikov G V, Hansch T W and Bloch I 2004 *Nature* **429** 277
[35] Kinoshita T, Wenger T and Weiss D S 2004 *Science* **305** 1125
[36] Girardeau M D and Minguzzi A 2007 *Phys. Rev. Lett.* **99** 230402
[37] Deuretzbacher F, Fredenhagen K, Becker D, Bongs K, Sengstock K and Pfannkuche D 2008 *Phys. Rev. Lett.* **100** 160405
[38] Zinner N T, Volosniev A G, Fedorov D V, Jensen A S and Valiente M 2014 *EPL* **107** 60003
[39] Olshanii M 1998 *Phys. Rev. Lett.* **81** 938
Haller E, Mark M J, Hart R, Danzl J G, Reichsöllner L, Melezhik V, Schmelcher P and Nägerl H-C 2010 *Phys. Rev. Lett.* **104** 153203
[40] Papp S B, Pino J M and Wieman C E 2008 *Phys. Rev. Lett.* **101** 040402
[41] Thalhammer G, Barontini G, De Sarlo L, Catani J, Minardi F and Inguscio M 2008 *Phys. Rev. Lett.* **100** 210402
[42] Garcia-March M A and Busch Th 2013 *Phys. Rev.* A **87** 063633
[43] Zöllner S, Meyer H-D and Schmelcher P 2008 *Phys. Rev.* A **78** 013629
[44] Hao Y J and Chen S 2009 *Phys. Rev.* A **80** 043608
[45] Hao Y J and Chen S 2009 *Eur. Phys. J. D* **51** 261–6
[46] Garcia-March M A, Juliá-Díaz B, Astrakharchik G E, Busch Th, Boronat J and Polls A 2013 *Phys. Rev.* A **88** 063604
[47] Deuretzbacher F, Becker D, Bjerlin J, Reimann S M and Santos L 2014 *Phys. Rev.* A **90** 013611
[48] He X, Xu P, Wang J and Zhan M 2010 *Opt. Express* **18** 13586
[49] Serwane F, Zürn G, Lompe T, Ottenstein T B, Wenz A N and Jochim S 2011 *Science* **332** 336
[50] Zürn G, Serwane F, Lompe T, Wenz A N, Ries M G, Bohn J E and Jochim S 2012 *Phys. Rev. Lett.* **108** 075303
[51] Wenz A N, Zürn G, Murmann S, Brouzos I, Lompe T and Jochim S 2013 *Science* **342** 457
[52] Bourgain R, Pellegrino J, Fuhrmanek A, Sortais Y R P and Browaeys A 2013 *Phys. Rev.* A **88** 023428
[53] Busch T, Englert B-G, Rzazewski K and Wilkens M 1998 *Found. Phys.* **28** 549
[54] Idziaszek Z and Calarco T 2006 *Phys. Rev.* A **74** 022712
[55] Kestner J P and Duan L-M 2007 *Phys. Rev.* A **76** 033611
[56] Pflanzer A C, Zöllner S and Schmelcher P 2009 *J. Phys. B: At. Mol. Opt. Phys.* **42** 231002
[57] Pflanzer A C, Zöllner S and Schmelcher P 2010 *Phys. Rev.* A **81** 023612
[58] Liu X-J, Hu H and Drummond P D 2010 *Phys. Rev.* A **82** 023619
[59] Blume D 2012 *Rep. Prog. Phys* **75** 046401
[60] Gharashi S E, Daily K M and Blume D 2012 *Phys. Rev.* A **86** 042702
[61] Harshman N L 2012 *Phys. Rev.* A **86** 052122
[62] D'Amico P and Rontani M 2014 *J. Phys. B: At. Mol. Opt. Phys.* **47** 065303
[63] Harshman N L 2014 *Phys. Rev.* A **89** 033633
[64] Sowinski T, Grass T, Dutta O and Lewenstein M 2013 *Phys. Rev.* A **88** 033607
[65] Volosniev A G, Fedorov D V, Jensen A S, Valiente M and Zinner N T 2013 arXiv:1306.4610
[66] Astrakharchik G E and Brouzos I 2013 *Phys. Rev.* A **88** 021602(R)
[67] Wilson B, Foerster A, Kuhn C C N, Roditi I and Rubeni D 2014 *Phys. Lett.* A **378** 1065
[68] Pagano G *et al* 2014 *Nat. Phys.* **10** 198
[69] Boronat J and Casulleras J 1994 *Phys. Rev.* B **49** 8920
[70] Alon O E, Streltsov A I and Cederbaum L S 2007 *Phys. Rev.* A **76** 062501
[71] Lindgren E J, Rotureau J, Forssén C, Volosniev A G and Zinner N T 2014 *New J. Phys.* **16** 063003